scientific reports

Check for updates

OPEN

Enhanced sperm isolation via bulk acoustic waves for high-throughput motility screening

Zahra Saeidpour, Mohammadjavad Bouloorchi Tabalvandani, Saeed Javadizadeh & Majid Badieirostami✉

The increasing infertility rate has become a worrying global challenge in recent years. According to the report of the World Health Organization, the male factor is responsible for over half of infertility cases, which includes the lack of desirable characteristics in sperm motility, morphology, and DNA integrity. In recent years, it has been shown that clinical methods including density gradient centrifugation cause damage to sperm DNA and besides being invasive, they are costly and time-consuming. In contrast, microfluidics has been used as a promising and non-invasive approach to manipulate biological cells. Here, by using the microvortices created by the oscillation of the bubbles caused by the bulk acoustic waves, we were able to trap sperms with less motility. In contrast, the highly motile sperms overcame the force of the microvortices and were guided to the outlet pool by following the channel boundaries. As a result, over 50% and 44% improvement in sperm progressive motility and viability, respectively, as well as 40% improvement in DNA integrity, were observed in the analysis of sperms retrieved from the output pool. In addition to being fast and non-invasive, the proposed device benefits from an easy method for sperms retrieval and does not require any preprocessing of the raw sperm sample.

Keywords Highly motile sperm, Microvortices, Bulk acoustic wave, Acoustofluidic

The increase in the rate of infertility, especially the malefactor which is responsible for 50% of infertility cases, has caused a significant increase in psychological distress among couples[1,2]. Various male factors can lead to infertility, the most important of which are low sperm concentration, low sperm motility, and abnormal morphology[3]. In the past decades, assisted reproductive technology (ART) has provided several clinical methods, including intrauterine insemination (IUI)[4], in-vitro fertilization (IVF)[5], and intra-cytoplasmic sperm injection (ICSI)[6]. In the IUI, the sperm sample is placed directly in the uterus[4]. In the IVF, which is the most common method, the egg is removed from the follicle and fertilized in a petri dish by mixing it with a sperm sample, and then the fertilized egg is transferred to the uterus[5]. In the ICSI, a specific sperm is injected directly into the egg's cytoplasm, which is the most invasive procedure[6].

Isolation of sperms with favorable characteristics for use in ART is very critical and will lead to an increase in fertility likelihood[7]. There are two common separation methods. The swim-up separation method is based on the sperm's ability to swim to the top of the medium inside a vial held at a 45-degree angle[8]. Another method is the density gradient centrifugation (DGC), which uses the density difference between abnormal and normal sperms to collect live and normal sperms at the bottom of the vial[9]. Despite being effective, these techniques can have potentially destructive effects on sperms such as DNA fragmentation and production of reactive oxygen species (ROS)[9,10]. Also practically, they are time-consuming and labor-intensive as well as being prone to personnel error which can ultimately lower the success rate of the treatment procedure[11]. On the contrary, microfluidic devices have provided more promising capabilities than these conventional methods in isolating sperms with enhanced motility[12], morphology[13], and DNA integrity[14,15]for downstream fertility procedures. Also, compared to conventional methods, microfluidics requires less semen sample volume, it is more sensitive while being less expensive, and offers parallel sample processing resulting in higher throughput[15].

Generally, sperm separation is performed in two ways, one inspired by the physiology of the female reproductive tract (FRT)[16]and the other by using unnatural external forces[17,18]. The methods inspired by the nature include active and passive mechanisms which can separate sperms based on motility[19,20], chemotaxis[21], thermotaxis[22], and rheotaxis[23,24]. Active mechanisms are based on surface charge[25], the ability to swim against a laminar flow[23], the response to a chemical substance[21], and thermal gradient[22]. Although active sorting provides flexibility in operation[26], it has some limitations in terms of parallelization of the scheme to achieve the desired

MEMS Lab, School of Electrical and Computer Engineering, College of Engineering, University of Tehran, Tehran, Iran. ✉email: mbadiei@ut.ac.ir

throughput. In passive mechanisms, the geometry of microchannels is inspired by the shape of the natural in vivo environment of the FRT[20], however, they lack sufficient throughput[11].

Sperm separation by optical methods[27], dielectrophoresis[28], magnetic forces[29], and acoustic waves[18,30]are grouped as the modalities using external forces, which have a higher throughput capacity for sorting[11]. Among the external forces, low-intensity acoustic waves are very suitable for biological separations due to the fact that they do not damage the cell membrane and DNA integrity[31]. Thus, two forces that are more commonly used in microfluidic devices are surface acoustic waves (SAW)[32,33]and bulk acoustic waves (BAW)[34,35].

The SAW is produced by interdigital transducers (IDT) that are patterned on a piezoelectric substrate and emit acoustic waves at the surface of the substrate. They can be operated in different frequency ranges between 20 and 150 MHz by changing the design of the IDT[36]. Gai et al. have isolated sperms with high DNA integrity by applying SAW angled at 30 degrees with respect to the fluid flow direction in order to sort sperms based on motility, size, and non-sphericality of the head[11]. Conversely, BAW can be used with a much lower frequency ranging from 0.1 to 10 MHz[37], where acoustic waves are produced by using piezoelectric ceramics in full contact with the microfluidic chip substrate. In contrast to SAW, it is very easy to use and cost-effective without complex fabrication. Also, in sorting by SAW, only cells near the bottom surface of the channel can be controlled, while BAW propagates in the volume and provides the ability to manipulate a larger number of cells. Recently, Xu et al. have successfully separated sperms from female DNA by using BAW[38]. In another study, Wan et al. were able to successfully extract sperm cells from forensic mock samples using bubble-based acoustic filtration[39]. The bubbles trapped in the sidewall structures were oscillated by using the BAW and disturbed the smooth flow of the liquid, causing the formation of two microvortices around each bubble by virtue of acoustic streaming[40].

Horseshoe structures were first proposed by Ahmed et al. to make a mixer[41]. Then Yazdi et al. used it for bacterial aggregation and biofilm formation[42]. The concept was later utilized for sequential trapping and transporting microparticles[43], and simultaneous rotation of large cells[44]. Though useful, the uncontrollability of the bubble and its expansion over time has been observed in our initial experiment (See supplementary Fig. S2 online) and reported in some earlier studies[41–43], which can interfere with the experiment and cause less effective performance, especially for trapping.

In this paper, we presented a novel acoustofluidic device based on the bubble oscillation created by BAW for isolating highly motile sperms with high DNA integrity. To avoid bubble uncontrollable growth, we blocked the same horseshoe structure presented by Ahmed et al[41]. so that the bubble falls inside a closed chamber and is well controlled. That combines the advantages of solid structures and oscillating microbubbles, demonstrating enhanced acoustic streaming at low input power, to overcome the limitations of each approach and enable practical applications[45]. This device works only based on the swimming velocity of sperm and its inherent behavior, and it was carefully designed to allow for output sperms retrieval. The function of microvortices and their location around the structure were simulated using COMSOL Multiphysics software. The motility, viability, and integrity of DNA were evaluated for the output sperms population. Also, this acoustofluidic chip does not need any initial preparation of the sample and in less than 10 min outputs adequate sperm count for extraction.

Materials and methods

Device fabrication

The microfluidic chip was fabricated from polydimethylsiloxane (PDMS) using a standard soft lithography approach. First, a chromium glass was spun coated with S1813 photoresist (Shipley, Marlborough, MA, USA), after that, soft baked at 110 °C for 1 min. Next, the target pattern was transferred to the coated glass using direct laser lithography (μpg101, Heidelberg Instruments, Germany), creating a very sharp-edged photomask. After development and etch, this photomask was then employed to define a pattern on a silicon mold that had been pre-coated with negative SU-8 photoresist (MicroChem, Newton, MA, USA).

To fabricate the chip from the mold, the PDMS polymer was combined with its corresponding curing agent in a ratio of 10:1 (Sylgard 184 silicone elastomer kit, Dow Corning, MI, USA), and after degassing in a vacuum chamber, it was slowly poured over the silicon mold and thermally cured at 75 °C for 20 min. Then the cured PDMS was slowly peeled off and the inlet/outlet of the chip was punched and carefully washed using acetone and isopropyl alcohol (IPA). Then the PDMS layer together with a clean glass slide was placed in the reactive ion etching chamber (RIE270, Yarnikan Saleh, Tehran, Iran) and was exposed for 45 s to oxygen plasma with a power of 25 W. The PDMS layer was then bonded onto the glass slide as the substrate and kept at 80 °C for 15 min to enhance the bonding strength. A piezoelectric transducer (PZT, FT-12 T-18.5E, Yuansheng Electronics Co. Ltd., China) of 21 mm radius and 1 mm thickness was attached to the glass slide adjacent to the PDMS structure using epoxy resin (Fig. 1a).

Chip and sample preparation

After bonding the chip, it was stored in a container filled with deionized (DI) water for 48 h so that the entire channel was filled with water but no longer as it would lead to the release of air trapped inside the horseshoe structures and as a result, we were no longer able to observe the microvortices at the specified frequency.

Raw human semen was procured from Sara Infertility Treatment Centre (Tehran, Iran). Informed consent was obtained from all participants. All experiments were performed in accordance with relevant guidelines, and regulations, and all experimental protocols were approved by University of Tehran. Prior to experimental characterizations, the microfluidic channels were filled with modified human tubal fluid (mHTF, Arina Rayan, Tehran, Iran) mixed with bovine serum albumin (BSA) with a final concentration of 5 mg/ml to prevent the adhesion of sperms to the channels. Using a micropipette, 20 μl of the inlet medium quickly was replaced with the human sperm sample. The flow was quickly stabilized and the sperms employed their inherent swimming and boundary-following behaviors to move forward along the channel. Before each experiment, raw sperm

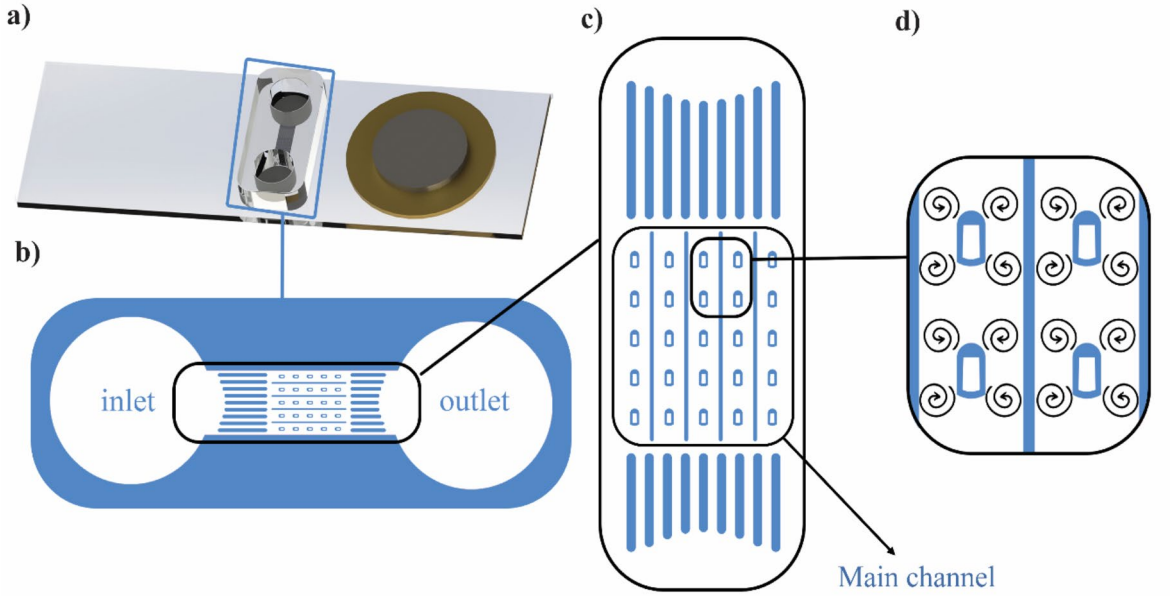

Fig. 1. (**a**) Picture of the entire device illustrating the PZT assembled on the glass slide next to the microfluidic chip. (**b**) Schematic of the microfluidic chip. (**c**) Enclosed horseshoe structures are located between a series of parallel channels for guiding motile sperms. Also, the main channel is located between the two groups of parallel channels at each end of the chip. (**d**) Generated microvortices in the vicinity of the horseshoe structures as a result of bubble oscillation. The wall thickness around the enclosed horseshoe structure is 30 μm.

characteristics including, concentration, viability, DNA fragmentation index (DFI), and motility were evaluated. Note that this method does not require any initial processing of the sperm sample like centrifugation or swim-up for instance, therefore it minimizes the damage to the sperms as well as it reduces the total time of the process.

Video recording and data analysis

Footage of sperm navigating through the chip was recorded by a Nikon Eclipse TS100 inverted microscope equipped with a Basler acA800-510uc camera at a rate of 100 fps. The trajectories of motile sperms were analyzed using an open-source computer-aided sperm analysis (OpenCASA) module within the ImageJ software. The parameters of Sperm motility parameters, such as straight-line velocity (VSL), linear curve velocity (VCL), average path velocity (VAP), linearity (LIN), and straightness (STR), were calculated from three separate trials to ensure the reliability of the data obtained. Statistical analysis was conducted using the student's *t*-test, with a significance level of $P \leq 0.05$.

Sperm DNA fragmentation assay

The assessment of sperm DNA integrity before and after separation was conducted using the sperm chromatin dispersion (SCD) assay (IVFCo, Tehran, Iran). SCD represents an indirect methodology for evaluating sperm DNA fragmentation. To start, the agarose gel was heated in boiling water for 10 min, followed by incubation at 37 °C for 5 min. Sperm samples were thoroughly blended with the agarose gel, and this mixture was evenly spread onto a glass slide, which was then covered with a coverslip. The slide was refrigerated at 4 °C for 5 min to allow the gel to set, after which the coverslip was carefully removed. Acid-unwinding solution (Solution A) was applied to the slide and incubated at room temperature for 7 min. Next, lysing solution (Solution B) was introduced and allowed to incubate for 15 min at room temperature. The slide was rinsed thoroughly with deionized water. Following the rinse, the sample underwent a gradual dehydration process using 70%, 90%, and absolute ethanol (Merck, Germany), each applied for 2 min. The sample was left to air-dry at room temperature before staining. Finally, the stained sample on the glass slide was analyzed under a microscope, where 100 sperm were counted to determine the DNA fragmentation index (DFI). Sperm cells exhibiting larger or medium-sized halos were classified as having intact DNA, whereas those with smaller halos or no halos were deemed to have fragmented DNA. This experiment was conducted with three distinct samples. (See supplementary Fig. S3 online)

Sperm vitality assay and concentration

To distinguish between live and dead sperm cells, the viability test by eosin-nigrosin staining (IVFCo, Tehran, Iran) was performed. Nigrosin creates a dark background to enhance clarity in visualization, while eosin affects only dead cells and renders them red. For this purpose, sperm sample was collected at the outlet, and was mixed with nigrosin and eosin at a ratio of 2:1:1 and left to sit at room temperature for 2 min. A thin layer of the mixture was applied onto a glass slide and 100 sperms were counted under the microscope to assess the viability.

To count the sperms, 20 µl of the sperm sample with 380 µl of diluting fluid solution (containing sodium bicarbonate) was mixed and loaded on a Neubauer chamber, then covered by a coverslip. Finally, the counted number was multiplied by 100,000 to get the sperm count in millions per millilitre.

Simulation

Finite element method using COMSOL Multiphysics v6.2 software was used to examine the time averaged streaming velocity field of microvortices, which was modeled through the pressure acoustics, the thermoviscous acoustics, and the laminar flow interface modules.

The investigation of the equations governing acoustic streaming induced by oscillating acoustic sources in a confined chamber has been the subject of thorough research[46–48]. Within this framework, we focus on a homogeneous isotropic fluid, and the equations governing continuity and momentum for the fluid flow can be expressed as follows[49]:

$$\frac{\partial \rho}{\partial t} + \nabla \cdot (\rho u) = 0 \tag{1}$$

$$\rho(\frac{\partial u}{\partial t} + u \cdot \nabla u) = -\nabla p + \mu \nabla^2 u + (\mu_b + \frac{1}{3}\mu)\nabla\nabla \cdot u = 0 \tag{2}$$

where u indicates the velocity field, ρ is the density of the fluid, µ is the dynamic viscosity, p is the pressure, t is the time, and $\mu_b$represent the bulk viscosity coefficient of the fluid. The presented model investigates the two-dimensional acoustic microvortices formed inside the microfluidic channel filled with water. The channel contains a single horseshoe structure positioned at the middle of the channel. The generation of acoustic streaming within the device is attributed to an acoustic body force, which is produced as a result of nonlinearities present in the Navier-Stokes equation[50]. The acoustic body force, denoted $\mathrm{F_{aco}}$, can be expressed as follows:

$$F_{aco} = -\nabla \cdot \langle \rho_0 v_{aco} v_{aco} \rangle = 0 \tag{3}$$

where the angle brackets denote the time-average of the parameters involved. To accurately capture the boundary layers oscillation by viscosity and thermal effects, as well as the acoustic body force, a refined mesh is required near the boundaries of the structure, and the thermoviscous acoustic model is employed.

The microvortices in question are generated through a nonlinear acoustic phenomenon known as acoustic streaming[51]. In mathematical terms, when considering the linearized first-order acoustic field of the Navier-Stokes equation,

$$\rho(u \cdot \nabla u) = -\nabla_p + \nabla \cdot \mu(\nabla u + (\nabla u)^T) \tag{4}$$

the resulting acoustic streaming field can be described as the time-averaged second-order field within the perturbation theory. Within the acoustic microvortices, the streaming effect is generated by nonlinear contributions near the boundaries of horseshoe structures inside the microfluidic channel.

The acoustic streaming domain coupling multiphysics feature is utilized to compute and apply the acoustic domain force to the laminar flow interface. This feature establishes a coupling between the thermoviscous acoustics frequency domain interface and the laminar flow interface. However, the complementary acoustic streaming boundary coupling, which is available for pressure acoustics and thermoviscous acoustics, is not employed in this particular setup as its contributions are considered negligible. The inclusion of the acoustic streaming boundary coupling would be only necessary when it is to accurately describe the resulting steady fluid flow.

Results and discussion

Chip design and sorting mechanism

Our microfluidic device was designed such that the flow rate was stable and zero, so no rheotaxis-based behavior was observed. Sperms were injected using a micropipette into the 6 mm-diameter inlet pool (Fig. 1b). The live motile sperms swam through the parallel channels (Fig. 1c) and shortly arrived in the main channel, where the separation mechanism initiated. Consequently, dead and non-motile sperms remained in the inlet pool and did not enter the main channel.

In the main channel, there are 5 identical rows of parallel channels each including 5 horseshoe structures in a row (Fig. 1c). Here, we proposed an enclosed horseshoe structure with a bubble trapped inside With improved stability compared to not enclosed bubbles (Fig. 1d). The total length of the chip is 1 cm, the width is 2.3 mm, including 460 µm for each row in the main channel and the height is 90 µm. Horseshoe structures are 180, 120, and 90 µm in length, width, and height, respectively, and are aligned in a row with an equal distance of 250 µm. At the end of the main channel, there are parallel channels with 130 µm width to guide the separated sperms into the outlet pool, which is also punched with a 6 mm hole so for the separated sperms to be extracted easily using a micropipette.

After the channels were filled with the sperm medium, the PZT was supplied with a voltage of 20 V_{pp}at the frequency of 164 kHz. The generated acoustic wave caused the bubbles trapped inside the enclosed horseshoe structures to oscillate and hence, to create microvortices in the surrounding fluid, known as acoustic streaming[40]. Exciting the bubble at its resonance frequency maximizes the efficiency of acoustic streaming. The resonance frequency can be approximated through the Rayleigh-Plesset equation[52,53]:.

$$f_0 = \frac{1}{2\pi r_b}\sqrt{\frac{3\gamma p_0}{\rho}} \tag{5}$$

where r_b is the radius of the bubble, γ is the polytropic exponent, p_0 denotes the ambient pressure and ρ is the density of the liquid. After this estimation, the resonance frequency is experimentally determined by sweeping the frequency range around the estimated frequency (for more information refer to the supplementary information ST1). The voltage value was discovered by comparing experimental results to achieve an optimal separation with high efficiency, which will be explained later.

The sperms that were able to reach the main channel act in two ways; some that never left the boundary of the main channel and preserved their boundary-following behavior, and the rest that came into the middle of the channel and consequently were trapped inside the microvortices. Among the trapped ones, some can reach to the peripheral microvortices, i.e., those having a high swimming velocity and being very motile, were able to escape the microvortices and migrate toward the channel sidewalls and eventually find a path to the exit (see supplementary video SV1 online). These behaviors are correlated with the higher DNA integrity of the very motile sperms compared to the rest[54]. On the contrary, less motile sperms were never able to overcome the microvortex force and were remained trapped (see supplementary video SV2 online).

Streaming flow simulation

Figure 2a illustrates the pressure field resulting from an actuation frequency of 164 kHz and an actuation displacement of 100 nm. Given that the amplitude of oscillation is relatively small, a perturbation expansion can be employed to describe the fluid flow components, such as density, pressure, and velocity, in the following manner[51]:

$$\rho = \rho_0 + \rho_1 + \rho_2 + \cdots \tag{6}$$

$$p = p_0 + p_1 + p_2 + \cdots \tag{7}$$

$$u = u_1 + u_2 + \cdots \tag{8}$$

The equations represented by (1) and (2) can be written in terms of static, first-order, and second-order quantities denoted by subscripts 0, 1, and 2, respectively. The higher-order terms which are not explicitly provided, can be safely ignored when calculating the first-order acoustic field and second-order acoustic streaming field. This is justified by their extremely small magnitudes, as confirmed by previous research[46].

The steady acoustic streaming flow is computed using the previously solved acoustic fields. The generation of the streaming flow is attributed to the presence of an acoustic body force, $\mathrm{F_{aco}}$ (Eq. (5)), in the proximity of the boundaries of the horseshoe structure. This effect is incorporated using the acoustic streaming domain coupling feature. The resulting velocity field is shown in Fig. 2b in a logarithmic scale to accurately represent the complex and fast flow around the horseshoe structure. The horseshoe structure creates two strong microvortices in both the front and in the rear parts. This simulation serves as a demonstration of how an acoustic field can induce a steady fluid flow in confined microfluidic systems. In Fig. 2c, sperm cells were stained using fluorescence dye for better visualization and the formation of microvortices is evident, which can effectively trap the sperms (see supplementary video SV3 online). The simulation results are in good agreement with the experimental observations (see supplementary video SV4 online).

Experimental results

After the injection, live and motile sperms quickly started swimming inside the parallel channels and by following the sidewalls, reached the main channel (see supplementary video SV5 online). This kind of design also helps to ensure that debris and residual components in the sample, such as white blood cells or dead sperms, do not enter the main channel. As shown in Fig. 3, the main channel was filled up after around three minutes. It is worth emphasizing that at the same time of the sperm injection, the PZT was also turned on so to emit the BAW.

Besides sperm swimming velocity, sperm cells were also affected by two forces, the drag force and the radiation force. The drag force caused by the acoustic streaming can be calculated using the Stokes' drag[49]:

$$F_{drag} = -6\pi\,\mu\, r_c v_c \tag{9}$$

where μ is the viscosity of the fluid, r_c is the radius of the sperm, and $v_c$is the relative velocity of the fluid and sperms. The acoustic radiation force that results from the scattering of the BAW by the oscillating bubble affects the particles located in the acoustic field as following[49]:

$$F_{rad} = -\pi\, r_c^{\,3}\left(\frac{2k_0}{3}\,Re\left[f_1{}^{*}p^{*}\nabla\, p\right] - \rho_{\,0} Re\left[f_2{}^{*}u^{*}\nabla\, u\right]\right) \tag{10}$$

where k_0 and $\rho_{\,0}$ are the compressibility and density of the fluid, respectively. f_1 and f_2 prefactors are dependent on fluid and cell characteristics, for more information refer to the supporting information ST3.

In general, small particles such as sperms are more affected by the drag force and thus pushed out to the edge of the microvortices (for more information see supplementary information ST4)[39]. In this way, each sperm has the opportunity to use its inherent swimming velocity to escape the microvortices and swim towards the channel wall, and used their boundary-following behavior to the exit. In contrast, sperms that have a low motility stay trapped in the microvortices. Therefore, sperm motility is the critical factor in this sorting process.

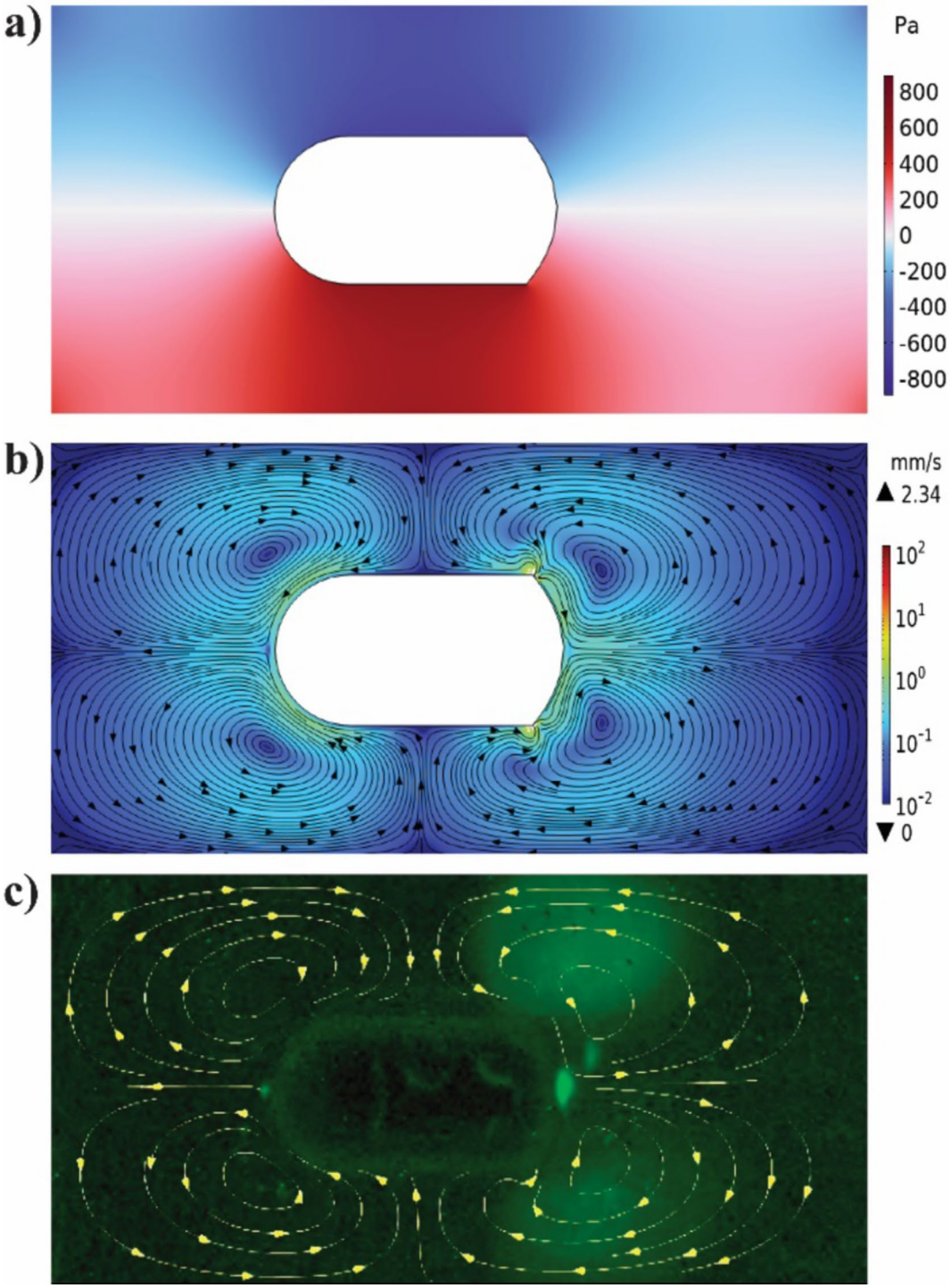

Fig. 2. (**a**) Acoustic pressure field in the microfluidic channel. (**b**) Steady streaming flow in the microfluidic channel driven by the acoustic source shows four vortices. (**c**) Experimental observation of vortices around the horseshoe structure (see supplementary information ST2). The highlighted green shows number of sperms inside the vortex that are stained with a fluorescent dye.

The trajectories of the highly motile sperms being able to escape the microvortices and also the trajectories of the trapped sperms with less motility are shown in Fig. 4a and b, respectively.

First, we repeated the tests in triplicate at each voltage of 10, 15, 20, and 25 V_{pp} and a constant frequency of 164 kHz, which was the resonance frequency of the bubble and it was obtained through experimental trials. We analyzed the average swimming velocity and the concentration of sperms in the outlet pool and compared against the raw sample (see Table 1).

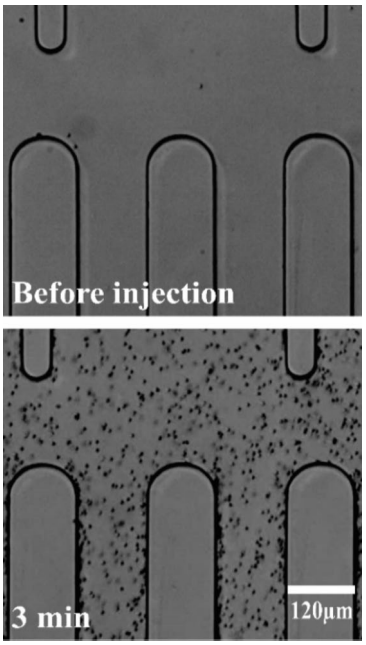

Fig. 3. The images above show a section of the guidelines, taken before and three minutes after the injection of sperms.

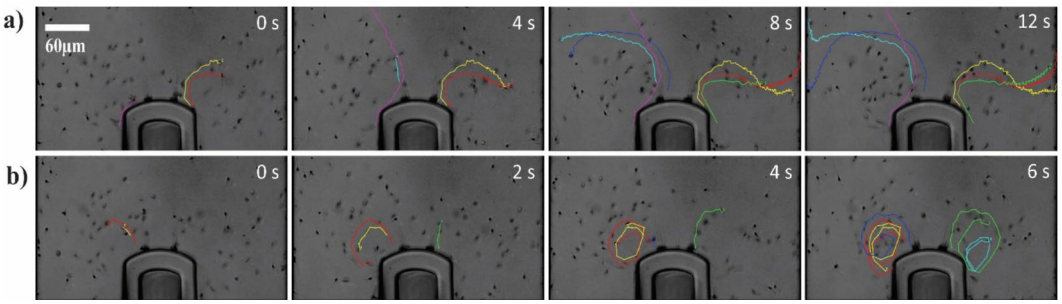

Fig. 4. The sperm trajectories with varying levels of motility in the vicinity of the generated microvortices. (**a**) Highly motile sperms after reaching the periphery of the vortices were able to escape and swim towards the channel wall. (**b**) The less motile sperms, trapped in the vortices rotating in a circular path with a velocity close to that of the vortices.

	Raw	10 V_{pp}	15 V_{pp}	20 V_{pp}	25 V_{pp}
VSL (µm/s)	23.5	29.3	37.1	48.2	56.2
VCL (µm/s)	73.2	89.9	98.2	104.5	144.8
VAP (µm/s)	43.9	50.4	50.5	58.3	75.5
LIN (%)	30.3	35.2	34.2	37	31.58
STR (%)	56.3	60	57.1	65.7	58.21
Concentration (M/ml)	50	1.22	0.17	0.11	0.028

Table 1. The average sperm kinematic parameters including straight-line velocity (VSL), curvilinear velocity (VCL), average path velocity (VAP), linearity (LIN), and straightness (STR) were calculated by openCASA. The average sperm concentration was also characterized using a Neubauer counting chamber.

Figure 5 shows the motility parameters calculated for the isolated sperms at different voltages compared against the raw sperm. The data clearly shows the monotonic increase of VSL, VAP, and VCL versus voltage. LIN, STR are also increased compared to the raw sample, however there is a relative decrease at 25 V_{PP}, which can be due to the increase in VAP and VCL as they have the opposite relationship. So, this is another reason for choosing 20 V_{PP} as the optimal voltage.

Figure 6a displays the exact same area of the outlet pool 8 min after the raw sample injection, at different excitation voltages. Figure 6b shows the quantitative values of sperm concentration versus excitation voltage. Though less number of sperms entering the outlet pool at higher voltages, they have superior swimming velocity parameters as listed in Table 1; Fig. 5. Considering the trade-off between concentration and motility of sperms collected in the outlet pool, the voltage of 20 V_{pp} was selected as the optimal performance point of the device. Besides sperm motility, sperm count is also a determining factor in a successful IVF process, and therefore it was considered for the selection of the optimal voltage. All experiments to measure vitality parameters and DNA fragmentation were performed at this excitation voltage.

Figure 7a shows the vitality for the isolated sperms versus the raw sperms. Based on the sperm vitality assay, nearly all the sperms collected in the outlet pool were viable (see supplementary video SV6 online). Figure 7b represents the sperms DNA fragmentation index (%DFI) for the isolated sperm versus the raw semen. The DNA fragmentation index (DFI) assesses sperm DNA integrity by measuring the percentage of sperms with fragmented DNA. The accepted threshold is 15–30% of DNA damage for a successful pregnancy, and values beyond 30% are considered to have poor integrity[55].

DNA integrity is an important and fundamental factor for fertility and for achieving the desired result from IVF methods[14]. Sperm with a high DNA integrity index will have a high chance of successful fertilization[56,57]. As seen in Fig. 7b for the isolated sperms, the DFI was 22 ± 1.5%, which is an obvious enhanced compared to the initial raw sample with a DFI of 63 ± 7.5%. The results show that no damage was done to the sperm during the separation process, and they will improve the quality necessary for use in artificial insemination and fertility operations.

From the 20 µL of the initial raw sample with an average concentration of 50 Million/ml, in less than 10 min, this device can retrieve around 5500 motile sperms in 50 µl of the extracted volume from the outlet pool. This is sufficient for IVF methods that need somewhere around 2000 to 10,000 sperms[58]. Also, is very easy to operate compared to other devices and methods that have been built and carried out so far specifically for the motile sperms retrieval.

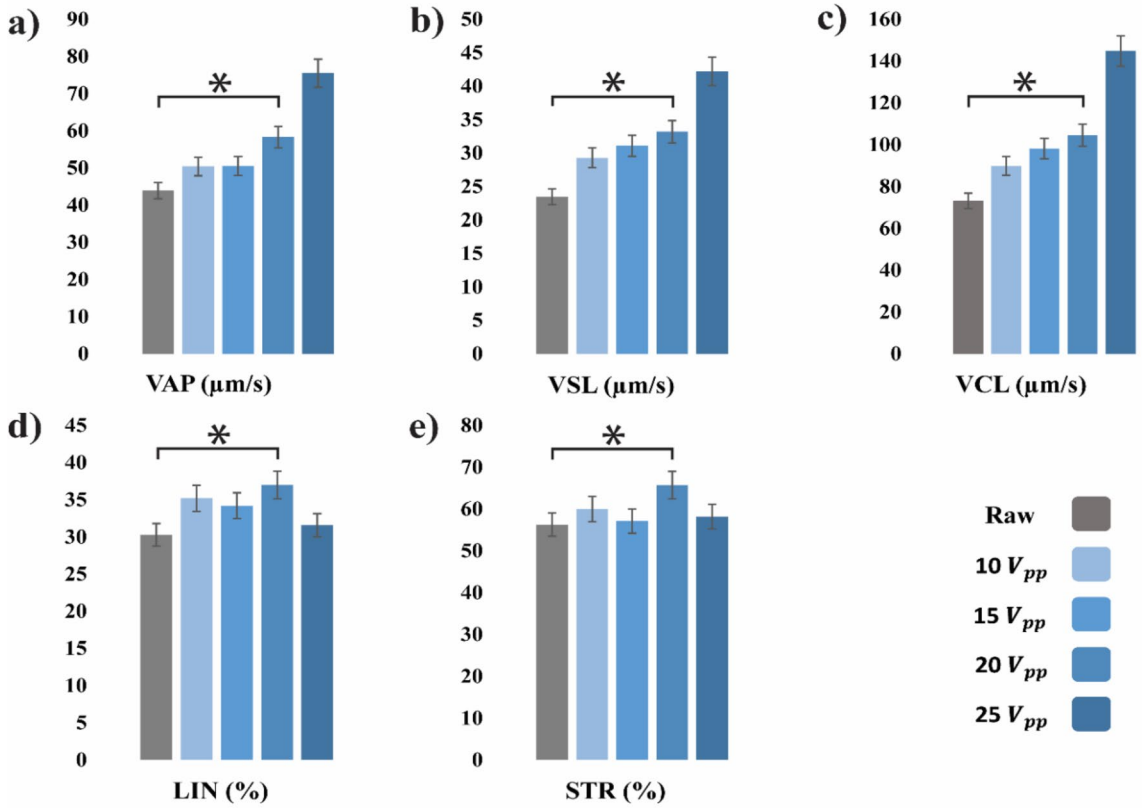

Fig. 5. Sperm kinematic parameters including (**a**) average path velocity (VAP), (**b**) straight-line velocity (VSL), (**c**) curvilinear velocity (VCL), (**d**) linearity (LIN), and (**e**) straightness (STR) for populations trapped in output pool compared to raw semen. Values are reported as mean ± standard deviation ($n = 3$), $^*P \leq 0.05$. The p-value is reported for the parameters at the optimal voltage versus the parameters of the raw sample.

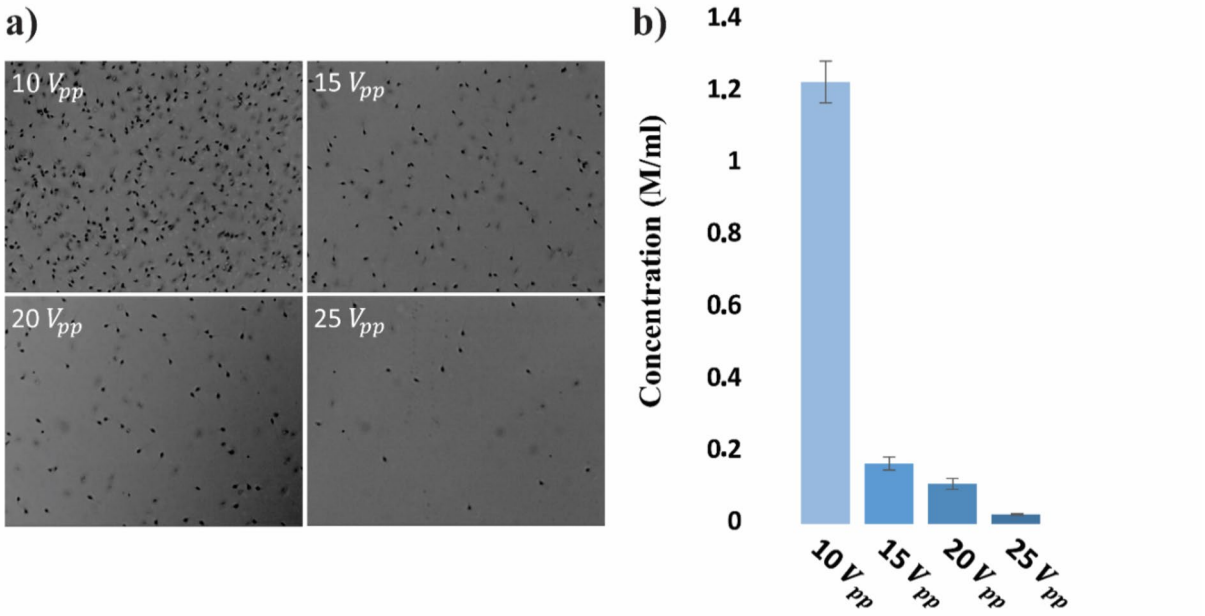

Fig. 6. (**a**) Population of isolated sperms in the outlet pool for different excitation voltages. The images were captured 8 min following the raw sample injection. (**b**) The concentration of sperms population in the outlet pool versus different voltages for an initial sample with a concentration of 50 Million/ml.

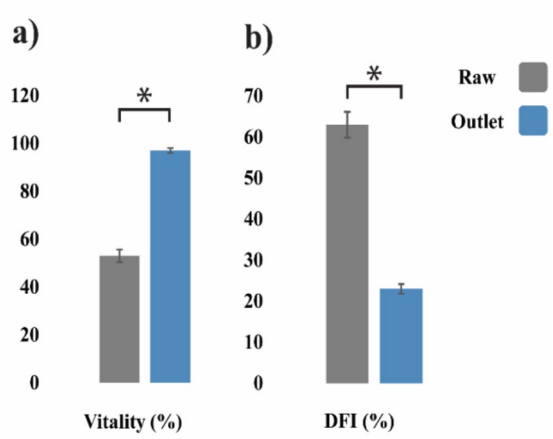

Fig. 7. (**a**) Vitality and (**b**) DNA fragmentation index (DFI) of the isolated sperms in the outlet pool compared with the raw sperms. Values are reported as mean ± standard deviation ($n = 3$), $^{*}P \leq 0.05$.

Conclusions

In this paper, we presented an acoustofluidic device to isolate highly motile sperms based on their swimming capability. It was shown that the highly motile sperms can overcome the force of the microvortices generated by the bubble oscillation and escape towards the outlet using their boundary-following behavior, which has been shown that nearly correlates with their superior DNA integrity. This device can isolate over 11,000 sperms in the total volume of the outlet pool with progressive motility and high DNA integrity in less than 10 min. Per the vitality tests and the DNA fragmentation assays, no damage seen as a result of acoustics manipulation of the sperms during the screening. The proposed device resulted in about 40% improvement in DNA integrity and about 50% and 44% improvements in progressive motility and viability, respectively.

Data availability

All data generated or analyzed during this study are available from the corresponding author on reasonable request. For more information see the supplementary information.

Received: 10 August 2024; Accepted: 31 October 2024

Published online: 04 November 2024

References

1. Winters, B. R. & Walsh, T. J. The epidemiology of male infertility. *Urol. Clin. North. Am.* **41**, 195–204 (2014).
2. Cao, D., Bai, C. & Zhang, G. Psychological distress among infertility patients: A Network Analysis. *Front. Psychol.* **13**, 906226 (2022).
3. Kumar, N. & Singh, A. Trends of male factor infertility, an important cause of infertility: a review of literature. *J. Hum. Reprod. Sci.* **8**, 191–196 (2015).
4. Aboulghar, M. et al. Intrauterine insemination. *Hum. Reprod. Update*. **15**, 265–277 (2009).
5. Wang, J. & Sauer, M. V. In vitro fertilization (IVF): a review of 3 decades of clinical innovation and technological advancement. *Ther. Clin. Risk Manag.* **2**, 355–364 (2006).
6. Seidman, D. G. & Kovacs The Subfertility Handbook: a clinician's guide. *J. Obstet. Gynecol. India*. **64**, 75–76 (2014).
7. Oseguera-López, I., Ruiz-Díaz, S., Ramos-Ibeas, P. & Pérez-Cerezales, S. Novel techniques of sperm selection for improving IVF and ICSI outcomes. *Front. cell. Dev. Biol.* **7**, 298 (2019).
8. Henkel, R. R. & Schill, W. B. Sperm preparation for ART. *Reprod. Biol. Endocrinol.* **1**, 108 (2003).
9. Malvezzi, H., Sharma, R., Agarwal, A., Abuzenadah, A. M. & Abu-Elmagd, M. Sperm quality after density gradient centrifugation with three commercially available media: a controlled trial. *Reprod. Biol. Endocrinol.* **12**, 121 (2014).
10. Zini, A., Finelli, A., Phang, D. & Jarvi, K. Influence of semen processing technique on human sperm DNA integrity. *Urology*. **56**, 1081–1084 (2000).
11. Gai, J., Nosrati, R. & Neild, A. High DNA integrity sperm selection using surface acoustic waves. *Lab. Chip*. **20**, 4262–4272 (2020).
12. Nallella, K. P., Sharma, R. K., Aziz, N. & Agarwal, A. Significance of sperm characteristics in the evaluation of male infertility. *Fertil. Steril.* **85**, 629–634 (2006).
13. Berkovitz, A. et al. The morphological normalcy of the sperm nucleus and pregnancy rate of intracytoplasmic injection with morphologically selected sperm. *Hum. Reprod.* **20**, 185–190 (2005).
14. Shamsi, M. B., Imam, S. N. & Dada, R. Sperm DNA integrity assays: diagnostic and prognostic challenges and implications in management of infertility. *J. Assist. Reprod. Genet.* **28**, 1073–1085 (2011).
15. Samuel, R. et al. Microfluidic-based sperm sorting & analysis for treatment of male infertility. *Transl Androl. Urol.* **7**, S336–S347 (2018).
16. Sakkas, D., Ramalingam, M., Garrido, N. & Barratt, C. L. R. sperm selection in natural conception: what can we learn from Mother Nature to improve assisted reproduction outcomes? *Hum. Reprod. Update*. **21**, 711–726 (2015).
17. Huang, J., Chen, H., Li, N. & Zhao, Y. Emerging microfluidic technologies for sperm sorting. *Eng. Regen*. **4**, 161–169 (2023).
18. Bouloorchi Tabalvandani, M. et al. Microfluidics as an emerging paradigm for assisted reproductive technology: a sperm separation perspective. *Biomed. Microdevices*. **26**, 23 (2024).
19. Tasoglu, S. et al. Exhaustion of racing sperm in nature-mimicking microfluidic channels during sorting. *Small*. **9**, 3374–3384 (2013).
20. Nosrati, R. et al. Rapid selection of sperm with high DNA integrity. *Lab. Chip.* **14**, 1142–1150 (2014).
21. Xie, L. et al. Integration of sperm motility and chemotaxis screening with a microchannel-based device. *Clin. Chem.* **56**, 1270–1278 (2010).
22. Doostabadi, M. R. et al. Microfluidic devices employing chemo- and thermotaxis for sperm selection can improve sperm parameters and function in patients with high DNA fragmentation. *Andrologia*. **54**, e14623 (2022).
23. Bouloorchi Tabalvandani, M., Javadizadeh, S. & Badieirostami, M. Bio-inspired progressive motile sperm separation using joint rheotaxis and boundary-following behavior. *Lab. Chip*. **24**, 1636–1647 (2024).
24. Bouloorchi, M., Javadizadeh, S., Valipour, A., Mousavi, M. & Badieirostami, M. Numerical study of a microfluidic-based motile sperm enrichment using sperm rheotaxis behavior. in *31st International Conference on Electrical Engineering (ICEE)* 484–487 (IEEE, 2023).
25. Ohta, A. T. et al. Motile and non-motile sperm diagnostic manipulation using optoelectronic tweezers. *Lab. Chip*. **10**, 3213–3217 (2010).
26. Nosrati, R., Gong, M. M., San Gabriel, M. C., Zini, A. & Sinton, D. Paper-based sperm DNA integrity analysis. *Anal. Methods*. **8**, 6260–6264 (2016).
27. Auka, N. et al. Optical tweezers as an effective tool for spermatozoa isolation from mixed forensic samples. *PLoS One*. **14**, e0211810 (2019).
28. Wongtawan, T., Dararatana, N., Thongkittidilok, C., Kornmatitsuk, S. & Oonkhanond, B. Enrichment of bovine X-sperm using microfluidic dielectrophoretic chip: a proof-of- concept study. *Heliyon*. **6**, e05483 (2020).
29. Gil, M., Sar-Shalom, V., Melendez Sivira, Y., Carreras, R. & Checa, M. A. Sperm selection using magnetic activated cell sorting (MACS) in assisted reproduction: a systematic review and meta-analysis. *J. Assist. Reprod. Genet.* **30**, 479–485 (2013).
30. Saeidpour, Z., Bouloorchi, M., Javadizadeh, S., Habibi, Z. & Badieirostami, M. Acoustofluidic-based motile sperm isolation using microvortices. in *30th National and 8th International Iranian Conference on Biomedical Engineering (ICBME)* 115–120 (IEEE, 2023).
31. Devendran, C., Carthew, J., Frith, J. E. & Neild, A. Cell adhesion, morphology, and metabolism variation via Acoustic exposure within Microfluidic Cell Handling systems. *Adv. Sci.* **6**, 1902326 (2019).
32. Lin, S. C. S., Mao, X. & Huang, T. J. Surface acoustic wave (SAW) acoustophoresis: now and beyond. *Lab. Chip*. **12**, 2766–2770 (2012).
33. Destgeer, G., Lee, K. H., Jung, J. H., Alazzam, A. & Sung, H. J. Continuous separation of particles in a PDMS microfluidic channel via travelling surface acoustic waves (TSAW). *Lab. Chip*. **13**, 4210–4216 (2013).
34. Neild, A., Oberti, S. & Dual, J. Design, modeling and characterization of microfluidic devices for ultrasonic manipulation. *Sens. Actuators B Chem.* **121**, 452–461 (2007).
35. Hill, M., Shen, Y. & Hawkes, J. J. Modelling of layered resonators for ultrasonic separation. *Ultrasonics*. **40**, 385–392 (2002).
36. Devendran, C., Albrecht, T., Brenker, J., Alan, T. & Neild, A. The importance of travelling wave components in standing surface acoustic wave (SSAW) systems. *Lab. Chip*. **16**, 3756–3766 (2016).
37. Laurell, T., Petersson, F. & Nilsson, A. Chip integrated strategies for acoustic separation and manipulation of cells and particles. *Chem. Soc. Rev.* **36**, 492–506 (2007).
38. Xu, K. et al. Isolation of a low number of sperm cells from female DNA in a Glass-PDMS-Glass microchip via bead-assisted acoustic Differential extraction. *Anal. Chem.* **91**, 2186–2191 (2019).
39. Wan, T. Y., Hwa, H. L., Lee, T. T. & Lu, Y. W. High efficiency sperm enrichment from forensic mock samples in bubble-based acoustic filtration devices for short tandem repeat (STR) analysis. *Lab. Chip*. **24**, 434–445 (2024).
40. Manasseh, R. Acoustic bubbles acoustic streaming, and cavitation microstreaming. in *Handbook of Ultrasonics and Sonochemistry* 1–36 (Springer Singapore, Singapore, 2015).
41. Ahmed, D., Mao, X., Shi, J., Juluri, B. K. & Huang, T. J. A millisecond micromixer via single-bubble-based acoustic streaming. *Lab. Chip*. **9**, 2738–2741 (2009).
42. Yazdi, S. & Ardekani, A. M. Bacterial aggregation and biofilm formation in a vortical flow. *Biomicrofluidics*. **6**, 044114 (2012).

43. Xie, Y. et al. Acoustofluidic Relay: sequential trapping and transporting of Microparticles via Acoustically Excited Oscillating bubbles. *J. Lab. Autom.* **19**, 137–143 (2014).
44. Tang, Q., Liang, F., Huang, L., Zhao, P. & Wang, W. On-chip simultaneous rotation of large-scale cells by acoustically oscillating bubble array. *Biomed. Microdevices*. **22**, 13 (2020).
45. Läubli, N. F. et al. Embedded microbubbles for Acoustic Manipulation of single cells and microfluidic applications. *Anal. Chem.* **93**, 9760–9770 (2021).
46. Lei, J., Glynne-Jones, P. & Hill, M. Comparing methods for the modelling of boundary-driven streaming in acoustofluidic devices. *Microfluid Nanofluidics*. **21**, 23 (2017).
47. Wiklund, M., Green, R. & Ohlin, M. Acoustofluidics 14: applications of acoustic streaming in microfluidic devices. *Lab. Chip*. **12**, 2438–2451 (2012).
48. Lei, J., Hill, M., de León Albarrán, C. P. & Glynne-Jones, P. Effects of micron scale surface profiles on acoustic streaming. *Microfluid Nanofluidics*. **22**, 140 (2018).
49. Muller, P. B., Barnkob, R., Jensen, M. J. H. & Bruus, H. A numerical study of microparticle acoustophoresis driven by acoustic radiation forces and streaming-induced drag forces. *Lab. Chip*. **12**, 4617–4627 (2012).
50. Muller, P. B. & Bruus, H. Numerical study of thermoviscous effects in ultrasound-induced acoustic streaming in microchannels. *Phys. Rev. E - Stat. Nonlinear Soft Matter Phys.* **90**, 043016 (2014).
51. Sadhal, S. S. & Acoustofluidics 13: Analysis of acoustic streaming by perturbation methods. *Lab Chip* 12, 2292–2300 (2012).
52. Leighton, T. G. & Apfel, R. E. *The acoustic bubble. J. Acoust. Soc. Am.* **96** (1994).
53. Minnaert, M. X. V. I. On musical air-bubbles and the sounds of running water. *Lond. Edinb. Dublin Philos. Mag J. Sci.* **16**, 235–248 (1933).
54. Eamer, L. et al. Turning the corner in fertility: high DNA integrity of boundary-following sperm. *Lab. Chip*. **16**, 2418–2422 (2016).
55. Li, F., Duan, X., Li, M. & Ma, X. Sperm DNA fragmentation index affect pregnancy outcomes and offspring safety in assisted reproductive technology. *Sci. Rep.* **14**, 356 (2024).
56. Duran, E. H., Morshedi, M., Taylor, S. & Oehninger, S. Sperm DNA quality predicts intrauterine insemination outcome: a prospective cohort study. *Hum. Reprod.* **17**, 3122–3128 (2002).
57. Muriel, L. et al. Value of the sperm deoxyribonucleic acid fragmentation level, as measured by the sperm chromatin dispersion test, in the outcome of in vitro fertilization and intracytoplasmic sperm injection. *Fertil. Steril.* **85**, 371–383 (2006).
58. Wu, J. K. et al. High-throughput flowing upstream sperm sorting in a retarding flow field for human semen analysis. *Analyst*. **142**, 938–944 (2017).

Acknowledgements

The authors would like to acknowledge Sara Infertility Center for providing human sperm samples for the experiments.

Author contributions

Z.S.: Conceptualized the idea, simulated the design, carried out experiments, and data analysis, and wrote the original manuscript. M.B.T.: Simulated the design, carried out experiments, editing, proofreading the manuscript. S.J.: carried out experiments. M.B.: Editing, proofreading the manuscript, and supervising the research. All authors reviewed the manuscript.

Declarations

Competing interests

The authors declare no competing interests.

Additional information

Supplementary Information The online version contains supplementary material available at https://doi.org/10.1038/s41598-024-78536-7.

Correspondence and requests for materials should be addressed to M.B.